

# The dynamics of co- and counter rotating coupled spherical pendulums

Blazej Witkowski<sup>1</sup>, Przemyslaw Perlikowski<sup>1,a</sup>, Awadhesh Prasad<sup>2</sup>, and Tomasz Kapitaniak<sup>1</sup>

<sup>1</sup> Division of Dynamics, Technical University of Lodz, 90-924 Lodz, Stefanowskiego 1/15, Poland

<sup>2</sup> Department of Physics and Astrophysics, University of Delhi, Delhi 110007, India

**Abstract.** The dynamics of co- and counter-rotating coupled spherical pendulums (two lower pendulums are mounted at the end of the upper pendulum) is considered. Linear mode analysis shows the existence of three rotating modes. Starting from linear modes allow we calculate the nonlinear normal modes, which are and present them in frequency-energy plots. With the increase of energy in one mode we observe a symmetry breaking pitchfork bifurcation. In the second part of the paper we consider energy transfer between pendulums having different energies. The results for co-rotating (all pendulums rotate in the same direction) and counter-rotating motion (one of lower pendulums rotates in the opposite direction) are presented. In general, the energy fluctuations in counter-rotating pendulums are found to be higher than in the co-rotating case.

## 1 Introduction

Coupled oscillators can exhibit complex phenomena such as: energy flows, synchronization, beating, internal resonances, amplitude death, chaotic and quasiperiodic transients etc. [1,2,3,4,5,6,7,8]. There are numerous studies on the dynamics of the single pendulum and coupled pendulums, but mostly devoted to in-plane oscillations [9,10,11]. In our studies we investigate the behavior of the coupled spherical pendulums. The first description of spherical pendulum dynamics has been presented by Olssen [12,13], who derived the equations of motion and solved them analytically using Lindstedt-Poincare method. The obtained solution shows periodic rotation of pendulum for small but finite displacements. The spherical pendulum is often taken as a model in quantum mechanics, for example in Refs. [14,15] where the authors consider a Hamiltonian system showing its asymptotic properties. In Ref. [16] the spherical pendulum is taken as an example to show different ways of solving Hamiltonian system with holonomic constrains. The authors show that the Penalty Method can compete with the Lagrange Multiplier Method and the choice of the method depends on the complexity of the problem and its expected accuracy. The dynamics of spherical pendulum for increasing value of energy is presented in Ref. [17] where

---

<sup>a</sup> e-mail: [przemyslaw.perlikowski@p.lodz.pl](mailto:przemyslaw.perlikowski@p.lodz.pl)

the authors consider several energy levels and present, using analytical and numerical tools, general scenarios of bifurcations. The global nonlinear stable manifolds of the spherical pendulum hyperbolic equilibrium with closed loop attitude control are analyzed by Lee *et al.* [18]. Their investigations have led us to understand the global stabilization properties of closed loop control systems on nonlinear spaces. The consequence of symmetry breaking including PT-transition is shown in Ref. [19]. The spherical pendulum is also used to model an arm carrying a cup of coffee [20].

The dynamics of double pendulum has been considered in Ref. [21] where the author used the model consisting of two rigid rods with elastic joints with the force acting parallel to lower pendulum. The detailed stability analysis based on the center manifold theorem has been considered for hanging down position. Then the periodic oscillations under the varying external force and damping coefficient have been studied. In another work [22] the general theory of Lagrangian reduction is applied to the equations of motion to simplify the problem and obtain the main form of vibrations and its bifurcations. The symmetric properties of spherical pendulum motion are investigated, in details, by Chossat and Bou-Rabee [23]. When the symmetry is present in the system one can observe a symmetric quasiperiodic and chaotic motions separated by heteroclinic connections. The analytical investigation including the analysis of double spherical pendulum topology was conducted by Hu *et al.* [24]. Their work has led us to understand the geometric as well as the dynamical properties of the systems.

In this paper we analyze the rotational motion of three coupled spherical pendulums. Using the linear approximation we obtain three independent linear modes of the pendulum's rotation. In each mode the pendulums rotate in clock-wise direction with different phase shifts and different amplitudes. Based on these linear modes we estimate nonlinear normal modes [25,26,27] using path-following algorithm. With the increase of total energy of the system the frequencies of the modes also increase. However, for higher energy level, the symmetry breaking pitchfork bifurcation occurs in first mode. For periodic solutions there is no transfer of energy between the pendulums. The energy flows among the pendulums for the co-rotating and counter-rotating rotations are discussed.

The paper is organized as follows. The considered model of the coupled spherical pendulum is introduced in Sec. 2. Sec. 3 contains the derivation of the eigenfrequencies and eigenvectors of the linearized systems, which let us compute the nonlinear normal modes. The energy flows between the pendulums are discussed in Sec. 4. The conclusions of the results are summarized in Sect. 5.

## 2 Model of two coupled spherical pendulums

We consider the system composed of an upper and two lower spherical pendulums as shown schematically in Fig. 1. The upper pendulum with mass  $M$  is suspended on weightless and inextensible string of length  $L$ . At the end of the upper pendulum two identical pendulums with mass  $m$  are suspended on weightless and inextensible strings of length  $H$ . The motion of upper pendulum is described by two angles  $\varphi$  and  $\theta$ , where  $\varphi$  is the angle between the string  $L$  and the plane  $YZ$ , while angle  $\theta$  represents the angular position of the pendulum around axis  $X$ . Motions of the first and the second lower pendulum are described in the same manner by variables  $\varphi_1, \theta_1$  and  $\varphi_2, \theta_2$  respectively. This system is Hamiltonian as there is neither external force nor dissipation of energy due to any type of frictional force.

In Cartesian coordinates the position of the upper pendulum can be written using transformation:  $x_0 = L \sin \varphi$ ,  $y_0 = L \sin \theta \cos \varphi$  and  $z_0 = -L \cos \theta \cos \varphi$ . Similarly, for each lower pendulum the coordinates can be written as follows:  $x_i = H \sin \varphi_i + x_0$ ,

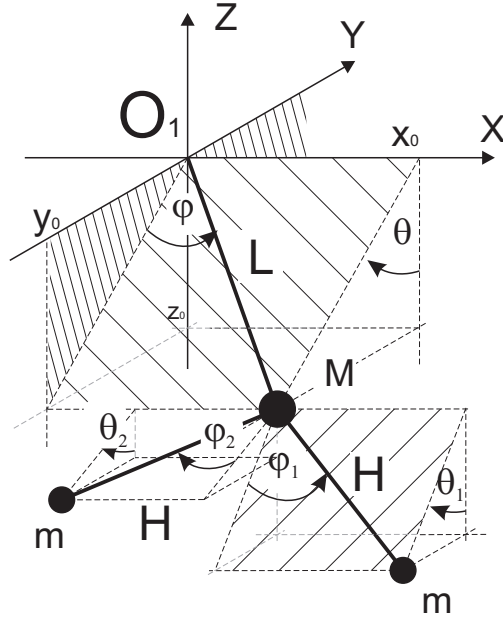


**Fig. 1.** Schematic figure for the coupled pendulum.

$y_i = H \sin \theta_i \cos \varphi_i + y_0$  and  $z_i = -H \cos \theta_i \cos \varphi_i + z_0$ , where  $i = 1, 2$ . The total kinetic energy is composed of the energy of the upper pendulum and the energy of two lower pendulums. For upper pendulum this energy is given by:

$$T_M = \frac{1}{2}M(\dot{x}_0^2 + \dot{y}_0^2 + \dot{z}_0^2) = \frac{1}{2}L^2M(\cos^2 \varphi \dot{\theta}^2 + \dot{\varphi}^2),$$

while the kinetic energy of the  $i$ -th lower pendulum can be expressed as:

$$\begin{aligned} T_{m_i} &= \frac{1}{2}m(\dot{x}_i^2 + \dot{y}_i^2 + \dot{z}_i^2) = \\ &= \frac{1}{2}m \left( L^2 \cos^2 \varphi \dot{\theta}^2 + H^2 \cos^2 \varphi_i \dot{\theta}_i^2 - 2HL \cos \varphi_i \sin[\theta - \theta_i] \sin \varphi \dot{\theta}_i \dot{\varphi} + L^2 \dot{\varphi}^2 + \right. \\ &\quad \left. + 2HL(\cos \varphi \cos \varphi_i + \cos[\theta - \theta_i] \sin \varphi \sin \varphi_i) \dot{\varphi} \dot{\varphi}_i + H^2 \dot{\varphi}_i^2 + \right. \\ &\quad \left. + 2HL \cos \varphi \dot{\theta} (\cos[\theta - \theta_i] \cos \varphi_i \dot{\theta}_i + \sin[\theta - \theta_i] \sin \varphi_i \dot{\varphi}_i) \right), \end{aligned}$$

where  $i = 1, 2$ . The potential energy of the system is:

$$V = g(L(2m + M)(1 - \cos \theta \cos \varphi) + Hm(2 - \cos \theta_1 \cos \varphi_1 - \cos \theta_2 \cos \varphi_2)).$$

The total energy of the system (Hamiltonian)  $\mathcal{H}$  is equal to the sum of kinetic and potential energies of three considered pendulums. Based on Lagrange equation of the second type one can derive six coupled second order ODEs. The equations of motion of the upper pendulum are

$$\begin{aligned}
& L \cos \varphi \left( gM \sin \theta - 2LM \sin \varphi \dot{\theta} \dot{\varphi} + LM \cos \varphi \ddot{\theta} + m \sum_{i=1}^2 \left( g \sin \theta + H \cos \varphi_i \sin[\theta - \theta_i] \dot{\theta}_i^2 - \right. \right. \\
& 2L \sin \varphi \dot{\theta} \dot{\varphi} - 2H \cos[\theta - \theta_i] \sin \varphi_i \dot{\theta}_i \dot{\varphi}_i + H \cos \varphi_i \sin[\theta - \theta_i] \dot{\varphi}_i^2 + L \cos \varphi \ddot{\theta} + \\
& \left. \left. H \cos[\theta - \theta_i] \cos \varphi_i \ddot{\theta}_i + H \sin[\theta - \theta_i] \sin \varphi_i \ddot{\varphi}_i \right) = 0, \tag{1}
\end{aligned}$$

and

$$\begin{aligned}
& L \left( gM \cos \theta \sin \varphi + LM \cos \varphi \sin \varphi \dot{\theta}^2 + LM \ddot{\varphi} + m \sum_{i=1}^2 \left( g \cos \theta \sin \varphi + L \cos \varphi \sin \varphi \dot{\theta}^2 + \right. \right. \\
& H \cos[\theta - \theta_i] \cos \varphi_i \sin \varphi \dot{\varphi}_i^2 - H \cos \varphi \sin \varphi_i \dot{\varphi}_i^2 + H \cos[\theta - \theta_i] \cos \varphi_i \sin \varphi \dot{\theta}_i^2 + \\
& H \ddot{\varphi}_i (\cos \varphi \cos \varphi_i + \cos[\theta - \theta_i] \sin \varphi \sin \varphi_i) + 2H \sin[\theta - \theta_i] \sin \varphi \sin \varphi_i \dot{\theta}_i \dot{\varphi}_i - \\
& \left. \left. H \sin[\theta - \theta_i] \cos \varphi_i \sin \varphi \ddot{\theta}_i + H \cos \theta \cos \varphi_i \sin \theta_i \sin \varphi \ddot{\varphi}_i + L \ddot{\varphi} \right) = 0. \tag{2}
\end{aligned}$$

The dynamics of the  $i$ -th lower pendulum is also described by two second order ODEs:

$$\begin{aligned}
& Hm \cos \varphi_i \left( g \sin \theta_i - 2H \sin \varphi_i \dot{\theta}_i \dot{\varphi}_i + H \cos \varphi_i \ddot{\theta}_i - L \left( \cos \varphi \sin[\theta - \theta_i] \dot{\theta}^2 + \right. \right. \\
& \left. \left. 2 \cos[\theta - \theta_i] \sin \varphi \dot{\theta} \dot{\varphi} + \cos \varphi (\sin[\theta - \theta_i] \dot{\varphi}^2 - \cos[\theta - \theta_i] \ddot{\theta}) + \sin[\theta - \theta_i] \sin \varphi \ddot{\varphi} \right) \right) = 0, \tag{3}
\end{aligned}$$

and

$$\begin{aligned}
& Hm \left( g \cos \theta_i \sin \varphi_i + L \cos[\theta - \theta_i] \cos \varphi \sin \varphi_i \dot{\theta}^2 + H \cos \varphi_i \sin \varphi_i \dot{\theta}_i^2 - \right. \\
& 2L \sin[\theta - \theta_i] \sin \varphi \sin \varphi_i \dot{\theta} \dot{\varphi} + L \left( (-\cos \varphi_i \sin \varphi + \cos[\theta - \theta_i] \cos \varphi \sin \varphi_i) \dot{\varphi}^2 + \right. \\
& \left. \left. \cos \varphi \sin[\theta - \theta_i] \sin \varphi_i \ddot{\theta} + (\cos \varphi \cos \varphi_i + \cos[\theta - \theta_i] \sin \varphi \sin \varphi_i) \ddot{\varphi} \right) + H \ddot{\varphi}_i \right) = 0, \tag{4}
\end{aligned}$$

where  $i = 1, 2$ . Eqs (1-4) describe the complete dynamics (without simplifications) of the system presented Fig. 1.

### 3 Nonlinear Normal Modes of the system

#### 3.1 Eigenfrequencies

For single spherical pendulum one can observe three modes which correspond to the periodic solutions. Two of them are rotational modes (symmetrical) and third is a planar mode where the pendulum swings in a vertical plane. In this paper we consider only rotational modes. For three coupled pendulums and low values of energy one can observe three rotational modes, each with own eigenfrequency (note that their mirror reflection are also present because of symmetry). To calculate these eigenfrequencies we apply the theory of linear normal modes. Let us assume that the amplitudes of motion of pendulums are small, hence we can consider that the system performs harmonic oscillations. To linearize the systems we use the following approximations:

$\sin \mathbf{q} = \mathbf{q}$  and  $\cos \mathbf{q} = 1$ , where  $\mathbf{q} = [\varphi, \theta, \varphi_1, \theta_1, \varphi_2, \theta_2]^T$ . For simplicity we can present the equations of motions, after linearization, in a matrix form:

$$\mathbf{A}\ddot{\mathbf{q}} + \mathbf{C}\mathbf{q} = 0, \quad (5)$$

where  $\mathbf{A}$  and  $\mathbf{C}$  are matrices of inertia and stiffness respectively, and they have got the following forms

$$\mathbf{A} = \begin{bmatrix} L^2(2m+M) & 0 & HLm & 0 & HLm & 0 \\ 0 & L^2(2m+M) & 0 & HLm & 0 & HLm \\ HLm & 0 & H^2m & 0 & 0 & 0 \\ 0 & HLm & 0 & H^2m & 0 & 0 \\ HLm & 0 & 0 & 0 & H^2m & 0 \\ 0 & HLm & 0 & 0 & 0 & H^2m \end{bmatrix}, \quad (6)$$

$$\mathbf{C} = \begin{bmatrix} gL(2m+M) & 0 & 0 & 0 & 0 & 0 \\ 0 & gL(2m+M) & 0 & 0 & 0 & 0 \\ 0 & 0 & gHm & 0 & 0 & 0 \\ 0 & 0 & 0 & gHm & 0 & 0 \\ 0 & 0 & 0 & 0 & gHm & 0 \\ 0 & 0 & 0 & 0 & 0 & gHm \end{bmatrix}. \quad (7)$$

For rotational modes, in three dimensional phase space, the periodic solutions are rotations around the hanging down position. For that reason we assume the solution of Eq. (5) as follows:

$$\mathbf{q} = \begin{bmatrix} \varphi \\ \theta \\ \varphi_1 \\ \theta_1 \\ \varphi_2 \\ \theta_2 \end{bmatrix} = \begin{bmatrix} \Psi_\varphi \sin[\omega t] \\ \Psi_\theta \cos[\omega t] \\ \Psi_{\varphi_1} \sin[\omega t] \\ \Psi_{\theta_1} \cos[\omega t] \\ \Psi_{\varphi_2} \sin[\omega t] \\ \Psi_{\theta_2} \cos[\omega t] \end{bmatrix} = \Psi \begin{bmatrix} \sin[\omega t] \\ \cos[\omega t] \\ \sin[\omega t] \\ \cos[\omega t] \\ \sin[\omega t] \\ \cos[\omega t] \end{bmatrix}, \quad \omega > 0, \quad t > 0, \quad \forall \Psi_{j=\{1,2,3\}} \in \mathbb{R}. \quad (8)$$

For linear oscillations of the system we observe the symmetry in two parallel planes (XY, YZ), hence  $\Psi_\varphi = \Psi_\theta$ ,  $\Psi_{\varphi_1} = \Psi_{\theta_1}$ ,  $\Psi_{\varphi_2} = \Psi_{\theta_2}$ . One can calculate the eigenfrequencies,  $\omega_{1,2,3}$ , for which the periodic solutions are observed in the system, using the relation  $(\mathbf{C} - \omega^2 \mathbf{A})\Psi = 0$ . The determinant  $\det |C - \omega^2 A|$  has to vanish, which gives three independent frequencies:

$$\omega_1 = \sqrt{\frac{g}{H}},$$

$$\omega_{2,3} = \sqrt{\frac{g}{L}} \sqrt{a \pm b}, \quad (9)$$

where  $a = \frac{(H+L)(2m+M)}{2HM}$  and  $b = \frac{\sqrt{2m+M} \sqrt{2(H+L)^2 m + (H-L)^2 M}}{2HM}$ .

The schematic representation of mode shapes corresponding to all three eigenfrequencies are shown in Fig. 2. Frequency  $\omega_1$  corresponds to the following solution: the phase shift between lower pendulums is  $\pi$ , which causes a balance of forces acting on the upper pendulum, hence the upper pendulum is at rest (see Fig. 2 (a)). For frequency  $\omega_2$  the upper and lower pendulums rotate in-phase, lower pendulums have the same amplitudes while the amplitude of upper pendulum is different (Fig. 2 (b)).

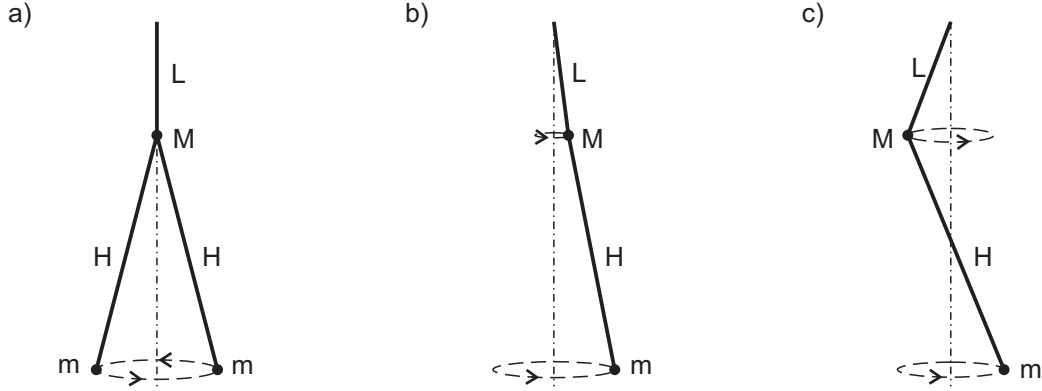


**Fig. 2.** The schematic representation of mode shapes for (a)  $\omega = \omega_1$  (b)  $\omega = \omega_2$  and (c)  $\omega = \omega_3$ .

For frequency  $\omega_3$  the phase of upper pendulum is shifted by  $\pi$  compared to the phases of both lower pendulums (Fig. 2 (c)).

The eigenvectors, corresponding the eigenfrequencies, can be written as:

$$\Psi_1 = [0, 0, \Psi_{\theta_1}, \Psi_{\theta_1}, -\Psi_{\theta_1}, -\Psi_{\theta_1}]^T,$$

$$\Psi_{2,3} = [\Psi_{\theta}, \Psi_{\theta}, \Psi_{\theta}(c \mp d), \Psi_{\theta}(c \mp d), \Psi_{\theta}(c \mp d), \Psi_{\theta}(c \mp d)], \quad (10)$$

where  $c = \frac{(H-L)(2m+M)}{4Hm}$  and  $d = \frac{\sqrt{2m+M}\sqrt{2(H+L)^2m+(H-L)^2M}}{4Hm}$ .

### 3.2 Nonlinear normal modes

In numerical calculations we assume the following values of system parameters:  $M = 2$ ,  $m = 2$ ,  $L = 1$ , and  $H = 3$ . After substituting these values in Eqs. (9) we obtain the following linear eigenfrequencies:  $\omega_1 = 1.732$ ,  $\omega_2 = 1.553$  and  $\omega_3 = 5.7959$ . Each of them describes the periodic solution of the linearized system. When we have applied one of them to the nonlinear system (Eqs (1, 2, 3, 4)), even assuming small energy, we obtain a quasiperiodic orbit (KAM tori) which is located close to the periodic solution of the linearized system. To correct the obtained solution, we have applied the Newton-Raphson algorithm. The integration of ODEs are performed with Runge-Kutta-Fehlberg (4,5) method. In Figure 3(a) we present, on the frequency - energy plot, how the frequencies of three periodic solutions change with the increase of the total energy  $\mathcal{H}$ . Each branch is calculated in the following way: for starting point ( $\mathcal{H} \approx 0.02$ ) we take initial conditions according to linear eigenvector, then we correct the obtained solution by Newton-Raphson scheme to periodic orbit. In next step this solution is perturbed (we add 1% of current total energy) so the energy is shifted to higher level and once again the correction is applied. The described procedure is repeated until the energy of the system reaches  $\mathcal{H} = 300$ . The successive increase of total energy  $\mathcal{H}$  causes the increase of three frequencies, hence the periods of rotations become shorter. The maximum value of energy can be  $\mathcal{H} = 300$  because for that value the system has singular point - the amplitude of upper pendulum reaches  $\pi/2$ . Therefore for branch No. 3 the maximum amplitude is close to  $\pi/2$ . Further increase of the energy ( $\mathcal{H} > 300$ ) for branches No. 1, 1a and 2 causes only the increase of the amplitude and the rotational velocity, but no new phenomena are observed.

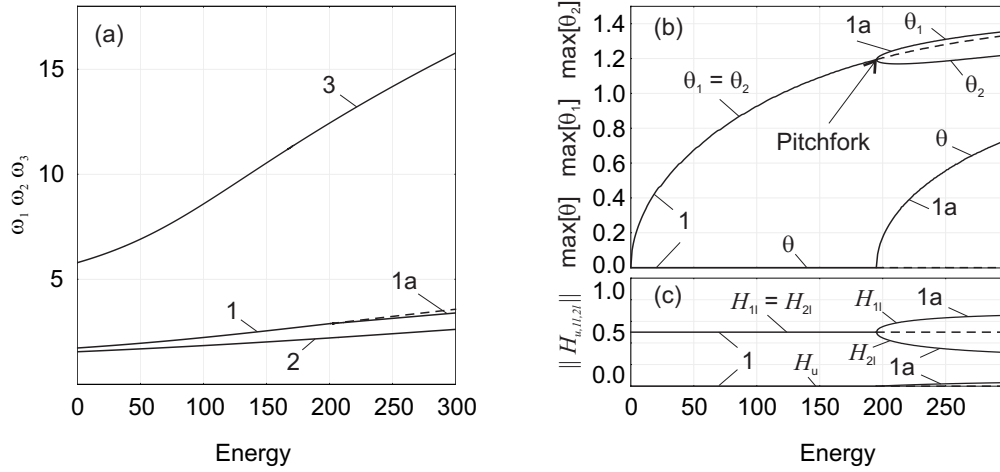


**Fig. 3.** (a) Frequency–energy plot of the investigated nonlinear system. Each branch begins with frequency calculated for linear system (No. 1 -  $\omega_1$ , No. 2 -  $\omega_2$  and No. 3 -  $\omega_3$ ). (b) The maximum amplitudes of solutions as a function of energy for branches No. 1 and No. 1a. At  $\mathcal{H} \sim 197$  we observe a pitchfork bifurcation which breaks the symmetry in the system, and hence the upper pendulum starts to oscillate ( $\theta \neq 0$ ) and amplitudes of lower pendulums ( $\theta_1$  and  $\theta_2$ ) have different values. (c) The normalized energies ( $\|\mathcal{H}\| = 1$ ) for each pendulum as a function of total energy of the system for branches No. 1 and No. 1a. The solid and dashed lines correspond to respectively stable and unstable periodic solutions.

Branch No. 1 corresponds to clock-wise rotations of lower pendulums with phase shifted by  $\pi$  while the upper one remains in hanging down position (see Fig. 2(a)). For energy level equal to  $\mathcal{H} = 197$  the symmetry breaking pitchfork bifurcation occurs. It is indicated by the appearance of No. 1a branch. After the bifurcation the frequencies of two solutions stay close in the whole range of considered energy. The changes of the maximum amplitudes of solutions along branches No. 1 and 1a are shown in Fig. 3(b). The solid and dashed lines correspond respectively to stable and unstable periodic solutions. For branch No. 1a, the oscillations of lower pendulums are asymmetric this causes that upper pendulum starts to oscillate increasing its amplitude with growing energy. The amount of energy in each pendulum for branches No. 1 and No. 1a is presented in Fig. 3(c). We normalize the total energy to one ( $\|\mathcal{H}\| = 1$ ) and show its participation in each pendulum. It is easy to see that for branch No. 1 the energy is equally distributed between lower pendulums. The upper pendulum is not moving before the bifurcation, hence its energy is equal to zero. For branch No. 1a the energy of first lower pendulum (energy  $\mathcal{H}_{1l}$ ) starts to increase while the energy of the second one decreases (energy  $\mathcal{H}_{2l}$ ). The energy of the upper pendulum also increases after the bifurcation.

The change of the shape of periodic orbits for branches No. 1 (black line) and No. 1a (grey line) are shown in Fig. 4. In upper and lower rows, the trajectories of upper pendulum and lower pendulums are presented respectively. For branch No. 1 the low energies solutions are nearly harmonic however for higher values of  $\mathcal{H}$  we observe the deformation around the maximum amplitude of pendulums. Therefore, the time when the pendulums are barely moving becomes longer in comparison to the rest period of oscillations. The periodic solution loses stability in the pitchfork bifurcation (the continuous line changes to the dashed one) and the asymmetric orbits appear (branch No. 1a).

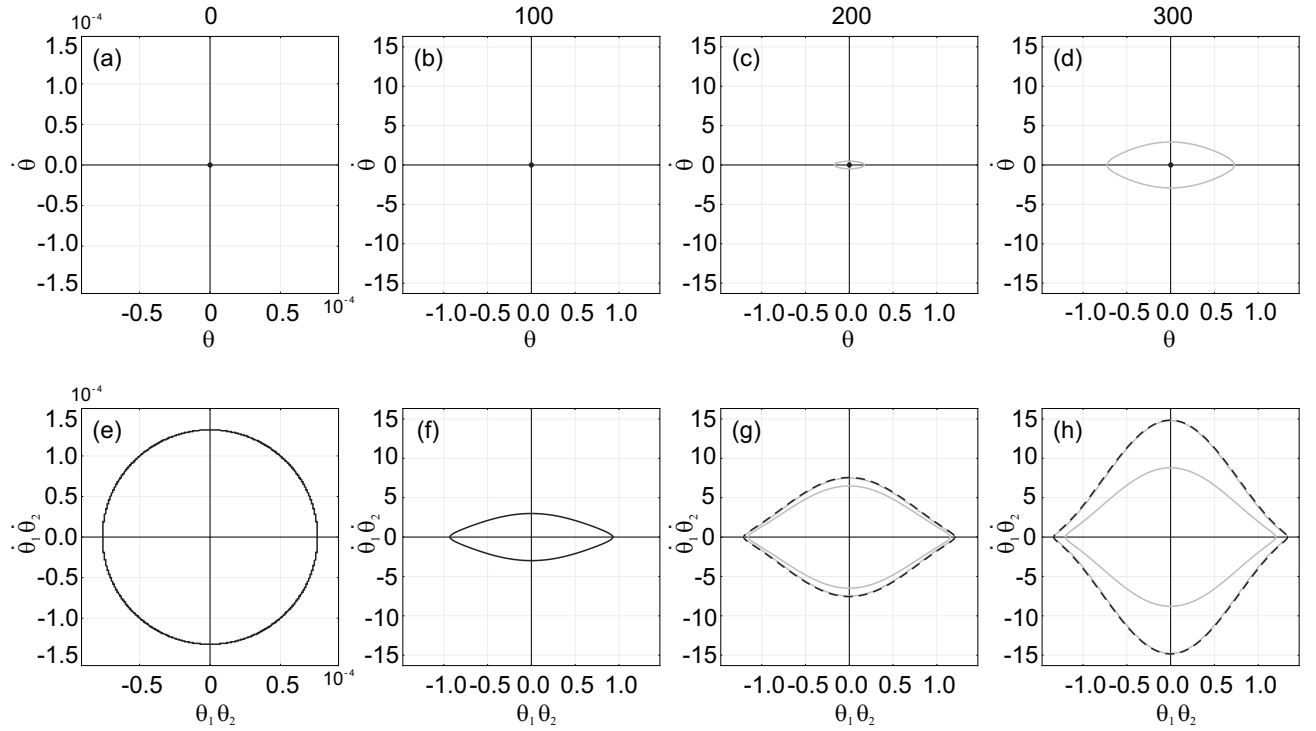


**Fig. 4.** The phase space trajectories of nonlinear normal modes along branches No. 1 and No. 1a. The total energy  $\mathcal{H}$  is increased from left to right:  $\mathcal{H} = 0.02$  (a,e),  $\mathcal{H} = 100$  (b,f),  $\mathcal{H} = 200$  (c,g) and  $\mathcal{H} = 300$  (d,h). The upper and lower rows show the motions of upper and lower pendulums respectively in phase space. The solid (stable solutions) and dashed (unstable solutions) black lines show periodic orbits along branch No. 1 while grey lines present the stable orbits along branch No. 1a.

For branch No. 2, corresponding to three pendulums oscillating in-phase, we observe a slow increase of oscillation amplitude with the increase of total energy. The periodic solutions along branch No. 2 change their shapes similar to branch No. 1 (not presented). For the third branch (No. 3) the upper pendulum rotates in anti-phase to lower pendulums. The changes of shape of periodic solutions are presented in Fig. 5. It is easy to see that, for low energy level, the orbits are nearly harmonic, while for higher levels of energy they become non-harmonic with visible nonlinear effects around the maximum amplitude. For  $\mathcal{H} = 300$  the maximum amplitude of upper pendulum reaches the singular point  $\theta = \pi/2$  (see Fig. 5(a)). In the case of branches No. 1 and No. 2 the amplitudes of lower pendulums increase much faster than the amplitude of the upper one, while for branch No. 3 we observe an opposite behavior.

## 4 Energy transfer among pendulums

In this section we present the energy transfer between lower pendulums via the upper pendulum. In the case of periodic solutions there is no energy transfer, i.e., the energy of each pendulum is constant. To observe the exchange of energy between the pendulums one has to perturb the periodic motion. This is done by introducing a small mismatch in the initial conditions. For low energy this leads to appearance of quasi-periodic motion (KAM tori) while for larger perturbations one can observe the



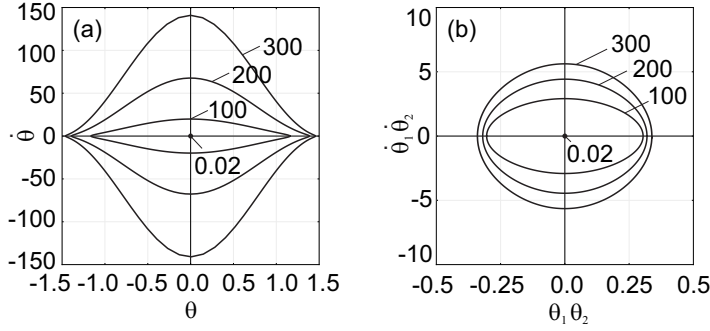


**Fig. 5.** The projections of trajectories in phase space of nonlinear normal modes of branch No. 3 for different energies:  $\mathcal{H} = 0.02$ ,  $\mathcal{H} = 100$ ,  $\mathcal{H} = 200$  and  $\mathcal{H} = 300$  of (a) upper and (b) lower pendulums.

chaotic behavior. Additionally, in this section we take into account counter-rotating solutions. To achieve these we change the sign of the initial velocities ( $\dot{\varphi}_2$  and  $\dot{\theta}_2$ ) of one of lower pendulums, i.e., forcing one pendulum to move in the opposite direction. As discussed below, we observe that all counter-rotating solutions are chaotic.

#### 4.1 Perturbation to first mode, $\omega_1$

For low level of the total energy ( $\mathcal{H} = 0.017035$ ) we take the following initial conditions:  $\theta = 0.0$ ,  $\varphi = 0.0$ ,  $\theta_1 = 0.012656702$ ,  $\varphi_1 = 0.0$ ,  $\theta_2 = -0.012656702$ ,  $\varphi_2 = 0.0$ ,  $\dot{\theta} = 0.0$ ,  $\dot{\varphi} = 0.0$ ,  $\dot{\theta}_1 = 0.0$ ,  $\dot{\varphi}_1 = 0.02192759$ ,  $\dot{\theta}_2 = 0.0$ ,  $\dot{\varphi}_2 = -0.02192759$ , which correspond to 1% perturbation of periodic solution. For counter-rotating the velocity of the second lower pendulum is equal to  $\dot{\varphi}_2 = 0.02192759$  (the velocity  $\dot{\theta}_2$  is equal to zero). In Fig. 6(a, e, i) we present how the energies of upper and lower pendulums change in time for co-rotating (black line) and counter-rotating (grey line) without additional perturbation. For co-rotating motion the pendulums do not transfer the energy between each other because of static upper pendulum, and synchronized periodic motions of lower pendulums. For counter-rotating motion the lower pendulums transfer energy via upper pendulum and motions are chaotic. For higher energy, after addition of small perturbation ( $\delta\theta_1 = 0.01\theta_1$  and  $\delta\varphi_1 = 0.01\varphi_1$ ) trajectories are shown in Fig. 6(b, f, j). In both cases, either co-rotating or counter-rotating, lower pendulums exchange energy via the upper pendulum. The co-rotating solution does not remain periodic but it becomes quasi-periodic. In quasi-periodic motion one can distinguish two independent frequencies - one of them remains from periodic motion the second one is responsible for modulation. This second frequency is much smaller than the frequency of original periodic orbit. This cause that we observe a slow transfer of energy. However the counter-rotating motion remains chaotic. Note that the energy is transferred with the same frequency but the amplitude of upper pendulum's motion is much higher for counter-rotating than for co-rotating.

In Fig. 6(c,g,k) we show the trajectories for high energy level, ( $\mathcal{H} = 101.468$ ) with the following initial conditions:  $\theta = 0.0$ ,  $\varphi = 0.0$ ,  $\theta_1 = 0.92996374$ ,  $\varphi_1 = 0.0$ ,  $\theta_2 = -0.92996374$ ,  $\varphi_2 = 0.0$ ,  $\dot{\theta} = 0.0$ ,  $\dot{\varphi} = 0.0$ ,  $\dot{\theta}_1 = 0.0$ ,  $\dot{\varphi}_1 = 1.79562871$ ,  $\dot{\theta}_2 = 0.0$ ,  $\dot{\varphi}_2 = -1.79562871$ . For counter-rotating case initial velocity of second pendulum is changed to  $\dot{\varphi}_2 = 1.79562871$ . The system behaves in similar way as in the low energy level cases. The only difference is in the amplitude of motion. However, for sufficiently high energy level, at ( $\mathcal{H} = 100$ ), as shown in Fig. 6(d, h, l), we observe higher energy transfer between pendulums for co-rotating case.

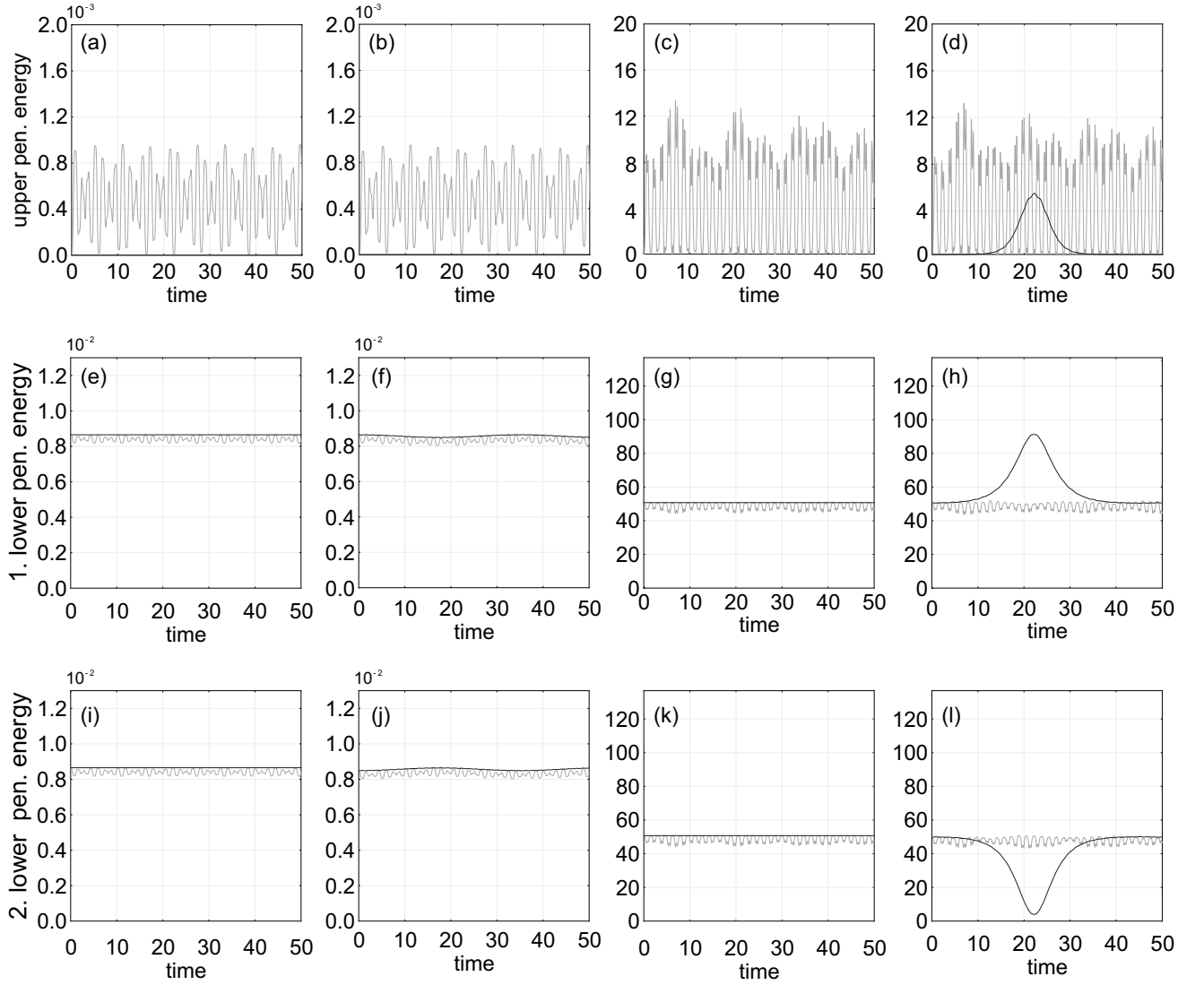


**Fig. 6.** The variation of energies as a function of time for the first mode,  $\omega_1$ . The figures of upper row (a-d) correspond to the upper pendulum while the lower two rows (e-l) are for lower pendulums. The black and grey lines in each figure represent co- and counter rotating solutions respectively. The trajectories for (a, e, i) low energy level with identical initial conditions, (b, f, j) low energy level with mismatched initial conditions, (c, g, k) high energy level ( $\mathcal{H} = 100$ ) with identical initial conditions, and (d, h, l) high energy level ( $\mathcal{H} = 100$ ) with mismatched initial conditions.

#### 4.2 Perturbation to second mode, $\omega_2$

For low energy level ( $\mathcal{H} = 0.0778345$ ) the following initial conditions are taken:  $\theta = 0.01745387$ ,  $\varphi = 0.0$ ,  $\theta_1 = 0.02384009$ ,  $\varphi_1 = 0.0$ ,  $\theta_2 = 0.02384009$ ,  $\varphi_2 = 0.0$ ,  $\dot{\theta} = 0.0$ ,  $\dot{\varphi} = 0.02710668$ ,  $\dot{\theta}_1 = 0.0$ ,  $\dot{\varphi}_1 = 0.03702315$ ,  $\dot{\theta}_2 = 0.0$ ,  $\dot{\varphi}_2 = 0.03702315$ . For counter-rotating solution the initial velocity of second pendulum is  $\dot{\varphi}_2 = -0.03702315$  (the velocity  $\dot{\theta}_2$  is equal to zero) is considered. In Fig. 7(a, e, i) we show the change of energies as a function of time for periodic motion for co-rotating and chaotic oscil-

lations for counter-rotating. For co-rotating case the pendulums do not transfer the energy between each other. The upper pendulum is moving in-phase with lower pendulums. When counter-rotating motion is observed lower pendulums transfer energy to upper pendulum and vice versa. The fluctuation in energy indicates that motions are chaotic.

Next we add the following perturbation to initial conditions:  $\delta\theta_1 = 0.01\theta_1$  and  $\delta\dot{\varphi}_1 = 0.01\dot{\varphi}_1$ . In Fig. 7(b, f, j) the change of energy in time for co-rotating and counter-rotating motions are presented. In both these cases lower pendulums exchange energy via the upper one. Energy is transferred with the similar frequency but the amount of the exchanged energy is much bigger for counter-rotating case than for co-rotating.

For higher energy level ( $\mathcal{H} = 100.989$ ) the following initial conditions are considered:  $\theta = 0.66836221$ ,  $\varphi = 0.0$ ,  $\theta_1 = 0.817659$ ,  $\varphi_1 = 0.0$ ,  $\theta_2 = 0.817659$ ,  $\varphi_2 = 0.0$ ,  $\dot{\theta} = 0.0$ ,  $\dot{\varphi} = 1.14578007$ ,  $\dot{\theta}_1 = 0.0$ ,  $\dot{\varphi}_1 = 1.3488661$ ,  $\dot{\theta}_2 = 0.0$ ,  $\dot{\varphi}_2 = 1.3488661$ . The trajectories are shown (Fig. 7(c, g, k)). For counter-rotating case the initial velocity of the second pendulum is changed to  $\dot{\varphi}_2 = -1.3488661$ . Counter-rotating solution continues to oscillate chaotically (Fig. 7(d, h, l)). In the co-rotating case lower pendulums oscillate in quasiperiodic way. However, for higher energy level ( $\mathcal{H} = 100.989$ ), the period of the energy transfer is much shorter than for lower energy level.

### 4.3 Perturbation to third mode, $\omega_3$

Now we consider the third mode where upper and lower pendulums move in opposite directions. For low energy level ( $\mathcal{H} = 0.0208567$ ) with the following initial conditions  $\theta = 0.017453269$ ,  $\varphi = 0.0$ ,  $\theta_1 = -0.0063880017$ ,  $\varphi_1 = 0.0$ ,  $\theta_2 = -0.0063880017$ ,  $\varphi_2 = 0.0$ ,  $\dot{\theta} = 0.0$ ,  $\dot{\varphi} = 0.10115284$ ,  $\dot{\theta}_1 = 0.0$ ,  $\dot{\varphi}_1 = -0.037024141$ ,  $\dot{\theta}_2 = 0.0$ ,  $\dot{\varphi}_2 = -0.037024141$  are taken. For counter-rotating solution we assume  $\dot{\varphi}_2 = 0.037024141$  (Fig. 8 (a, e, i)) Co-rotating solution is periodic and pendulums do not exchange energy between each other. In counter-rotating case we can observe a chaotic beating. Similar behavior is observed for higher energy level ( $\mathcal{H} = 100.898$ ) as shown in Fig. 8 (b,f,g). and  $\delta\dot{\varphi}_1 = 0.01\dot{\varphi}_1$ . The more energy transfer is in the counter-rotating oscillations than in co-rotating.

At high energy level ( $\mathcal{H} = 100.898$ ) with initial conditions:  $\theta = 1.16073984$ ,  $\varphi = 0.0$ ,  $\theta_1 = -0.32498693$ ,  $\varphi_1 = 0.0$ ,  $\theta_2 = -0.32498693$ ,  $\varphi_2 = 0.0$ ,  $\dot{\theta} = 0.0$ ,  $\dot{\varphi} = 7.90726534$ ,  $\dot{\theta}_1 = 0.0$ ,  $\dot{\varphi}_1 = -2.75298937$ ,  $\dot{\theta}_2 = 0.0$ ,  $\dot{\varphi}_2 = -2.75298937$  (Fig. 8(c, g, k)). For counter-rotating case, the initial velocity of second pendulum is changed to  $\dot{\varphi}_2 = 2.75298937$ . In these both cases, co- and counter-rotating oscillations of pendulums are chaotic for higher total energy level (Fig. 8(d, h, l)).

## 5 Summary

In this paper we study the dynamics of three coupled conservative spherical pendulums. The analytical calculations of the eigenfrequencies of the linearized system, allow us to identify three independent linear modes of the pendulum's rotation. For all of them, pendulums rotate in clock-wise direction with different phase shifts. The obtained linear modes allow us to compute the nonlinear normal modes for increasing energy in the system using the path-following method. As it is expected with growing total energy the frequencies of modes increase. In the first mode we observe a pitch-fork bifurcation, which causes the appearance of symmetry broken periodic solution and destabilization of the initial one.

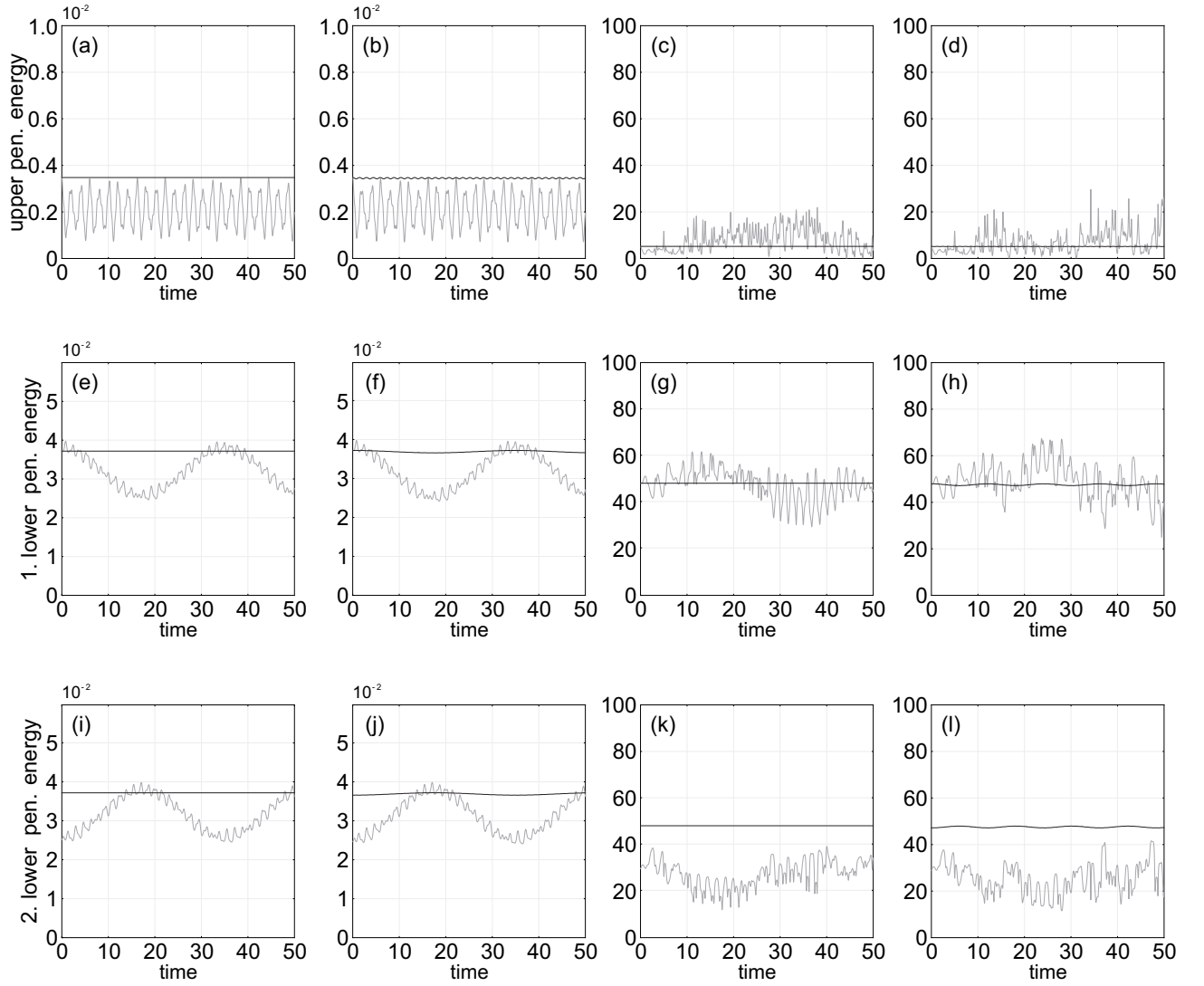


**Fig. 7.** The variation of energies as a function of time for the second mode,  $\omega_2$ . The figures of upper row (a-d) correspond to the upper pendulum while the lower two rows (e-l) are for lower pendulums. The black and grey lines in each figure represent co- and counter rotating solutions respectively. The trajectories for (a, e, i) low energy level with identical initial conditions, (b, f, j) low energy level with mismatched initial conditions, (c, g, k) high energy level ( $\mathcal{H} = 100.989$ ) with identical initial conditions, and (d, h, l) high energy level ( $\mathcal{H} = 100.989$ ) with mismatched initial conditions.

In the case of periodic motion there is no energy transfer between the pendulums, but even a small perturbation of periodic initial conditions leads to the exchange of energy. We show the energy flows for each mode considering two cases of rotations - in clock-wise and counter clock-wise directions. In the first case for all three modes we observe the dynamics on a KAM tori. The period of energy transfer is much longer than the natural period of each mode. In the second case the dynamics is always chaotic.

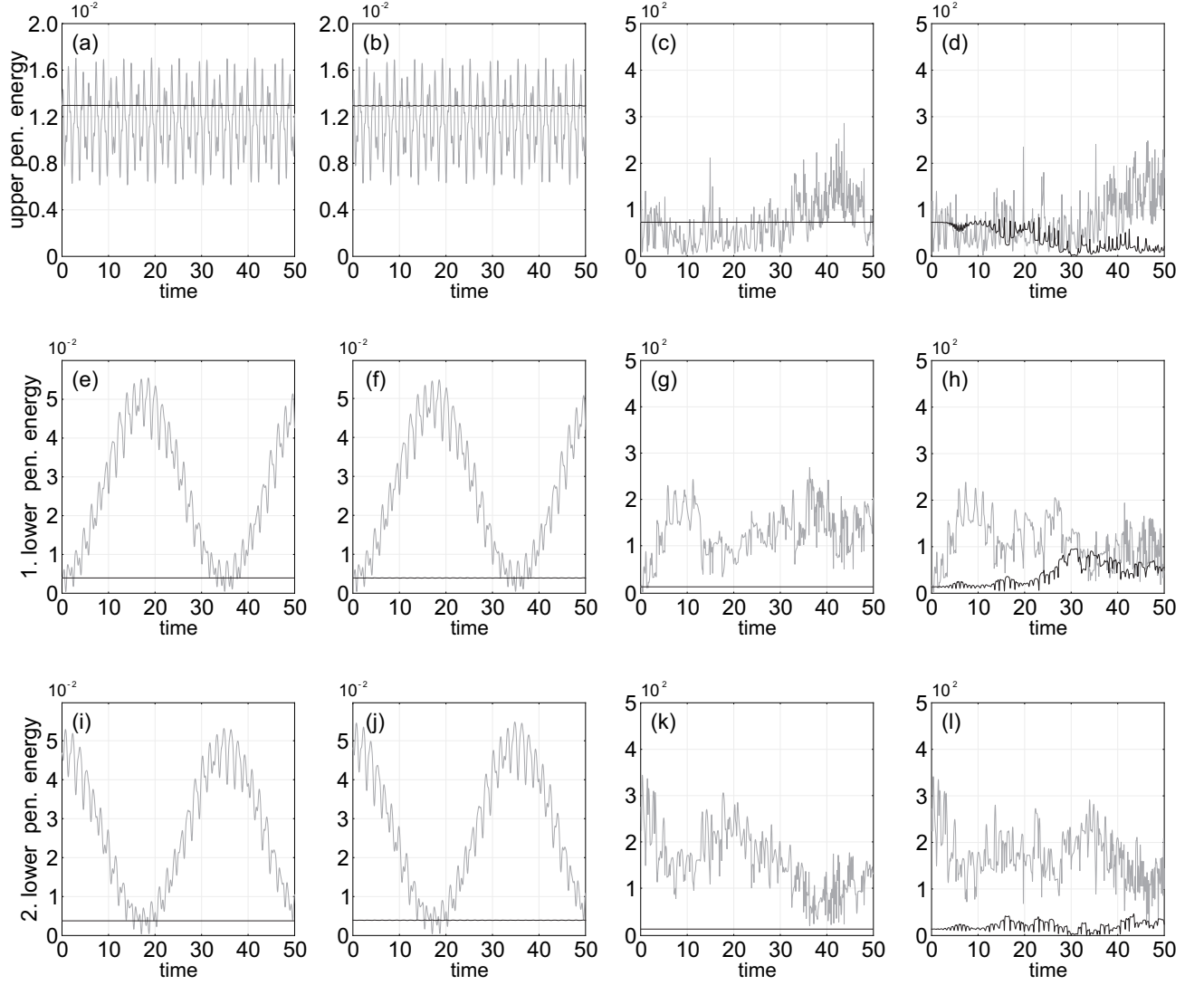


**Fig. 8.** The variation of energies as a function of time for the third mode,  $\omega_3$ . The figures of upper row (a-d) correspond to the upper pendulum while the lower two rows (e-l) are for lower pendulums. The black and grey lines in each figure represent co- and counter rotating solutions respectively. The trajectories for (a, e, i) low energy level with identical initial conditions, (b, f, j) low energy level with mismatched initial conditions, (c, g, k) high energy level ( $\mathcal{H} = 100.898$ ) with identical initial conditions, and (d, h, l) high energy level ( $\mathcal{H} = 100.898$ ) with mismatched initial conditions.

## Acknowledgments

This work has been supported by the Foundation for Polish Science, Team Programme under project TEAM/2010/5/5 (BW, PP, TK). AP would like to thank the DST, Govt. of India for financial support.

## References

1. A. Pikovsky, M. Rosenblum, J. Kurths, Cambridge University Press, 2001
2. S. H. Strogatz, *Physica D: Nonlinear Phenomena* **143**, 2000 1
3. Y. Kuramoto, Springer, 1984
4. S. Sabarathinam, K. Thamilmaran, L. Borkowski, P. Perlikowski, P. Brzeski, A. Stefanski, T. Kapitaniak, *Communications in Nonlinear Science and Numerical Simulation* **18**, 2013 3098
5. S. Yanchuk, K. Schneider, *Proceedings of Equadiff 2003* (World Sci.,2005) 494-496
6. A. Vakakis, O. Gendelman, L. Bergman, D. McFarland, G. Kerschen, Y. Lee, Springer **156**, 2008
7. G. Saxena, A. Prasad, R. Ramaswamy, *Physics Reports* **521**, 2012 205
8. N. E. Wierschem, D. D. Quinn, S. A. Hubbard, M. A. Al-Shudeifat, D. M. McFarland, J. Luo, L. A. Fahnestock, B. F. S. Jr., A. F. Vakakis, L. A. Bergman, *Journal of Sound and Vibration* **331**, 2012 5393
9. G. Rega, S. Lenci, B. Horton, M. Wiercigroch, E. Pavlovskaja, *International Journal of Bifurcation and Chaos* **22**, 2012 1250100
10. K. Czolczynski, P. Perlikowski, A. Stefanski, T. Kapitaniak, *Chaos: An Interdisciplinary Journal of Nonlinear Science* **21**, 2011
11. P. Brzeski, P. Perlikowski, S. Yanchuk, T. Kapitaniak, *Journal of Sound and Vibration* **331**, 2012 5347
12. M. G. Olsson, *American Journal of Physics* **46**, 1978 1118
13. M. G. Olsson, *American Journal of Physics* **49**, 1981 531
14. R. Cushman, J. J. Duistermaat, *Bulletin (New Series) of the American Mathematical Society* **19**, 1988 475
15. V. Guillemin, A. Uribe, *Communications in Mathematical Physics* **122**, 1989 563
16. S. Leyendecker, P. Betsch, P. Steinmann, *Computational Mechanics* **33**, 2004 174
17. P. H. Richter, H. R. Dullin, H. Waalkens, J. Wiersig, *The Journal of Physical Chemistry* **100**, 1996 19124
18. T. Lee, M. Leok, N. Harris McClamroch, *ArXiv e-prints*, [arXiv:1103.2822](https://arxiv.org/abs/1103.2822), 2011
19. C. M. Bender, B. K. Berntson, D. Parker, E. Samuel, *American Journal of Physics* **81**, 2013 173
20. H. C. Mayer, R. Krechetnikov, *Phys. Rev. E* **85**, 2012 046117
21. A. Steindl, H. Troger, *Bifurcation: Analysis, Algorithms, Applications* (Birkhauser Basel, 1987) 277-287
22. J. E. Marsden, J. Scheurle, *Zeitschrift fur angewandte Mathematik und Physik ZAMP* **44**, 1993 17
23. P. Chossat, N. Bou-Rabee, *SIAM Journal on Applied Dynamical Systems* **4**, 2005 1140
24. S. Hu, E. Leandro, M. Santoprete, *Regular and Chaotic Dynamics* **17**, 2012 36
25. S. Shaw, C. Pierre, *Journal of Sound and Vibration* **164**, 1993 85
26. G. Kerschen, M. Peeters, J.-C. Golinval, A. F. Vakakis, *Mechanical Systems and Signal Processing* **23**, (2009) 170
27. M. Peeters, R. Vignié, G. Sérandour, G. Kerschen, J.-C. Golinval, *Mechanical systems and signal processing* **23**,(2009) 195